

Anomalous hot electron generation via stimulated Raman scattering in plasma with up-ramp density profiles

Xuyan Jiang^{1,2}, Suming Weng^{1,2}, Hanghang Ma^{1,2}, Charles F. Wu^{1,2}, Zhao Liu^{1,2}, Min Chen^{1,2}, Bengt Eliasson³, Zhengming Sheng^{1,2,4*}

¹Key Laboratory for Laser Plasmas (MoE), School of Physics and Astronomy, Shanghai Jiao Tong University, Shanghai 200240, China

²Collaborative Innovation Center of IFSA, Shanghai Jiao Tong University, Shanghai 200240, China

³ SUPA, Department of Physics, University of Strathclyde, Glasgow, UK

⁴Tsung-Dao Lee Institute, Shanghai Jiao Tong University, Shanghai 200240, China

*Email: zmsheng@sjtu.edu.cn

ABSTRACT

The evolving electron plasma waves (EPWs) excited by stimulated Raman scattering (SRS) can generate anomalous energetic electrons in an inhomogeneous plasma with a positive density gradient. We investigate the evolution and propagation features of the EPW in the inhomogeneous plasma theoretically and confirmed with particle-in-cell simulations. It is found that the evolution of the EPW wavenumber is mainly related to the plasma density profile rather than the electron plasma temperature. When the density gradient is positive in the direction of the EPW propagation, the wavenumber of the EPW decreases with time and its phase velocity increases continuously, causing the trapped electrons to be further accelerated to anomalous high energy. Furthermore, it is found that the Langmuir decay instability tends to reduce the levels of SRS saturation and electron acceleration and produce hot electrons in the opposite direction. This work provides a new understanding of electron heating due to SRS excitation.

I. INTRODUCTION

Laser plasma instabilities (LPIs) are well-known to be one of the key issues in different schemes of laser-driven inertial confinement fusion (ICF) [1-3]. Tremendous progresses have been made in our understanding of the nonlinear development of LPIs and their mitigation [4-7]. One of the main LPIs is the stimulated Raman scattering (SRS), the decay of an incident laser into an electron plasma wave (EPW) and a scattered light [8, 9], which plays a prominent role in laser-plasma coupling. In particular, it produces hot electrons by the excited electron plasma waves (EPWs) [10, 11], which are generally detrimental to target compression. Considerable research efforts have been devoted to the suppress SRS [12-14]. Once the EPWs are excited via SRS, the Langmuir decay instability (LDI) is prone to occur [15, 16], where the EPW decays into a counterpropagating EPW and an ion acoustic wave. The LDI is considered as one of the saturation mechanisms of SRS [17, 18].

The generation of hot electrons by SRS may involve multiple stages. Usually, the phase velocity of the EPW excited by the backward-SRS (BSRS) is low and close to the electron thermal velocity. Therefore, many electrons can be trapped and heated by BSRS-induced EPWs, typically to the kinetic energy lower than 100keV [19, 20]. Meanwhile, the phase velocity of the forward-

SRS (FSRS)-induced EPW is typically much higher than the electron thermal velocity, so the electrons are hard to be trapped and accelerated by this EPW [21, 22]. In early studies, the idea of two-stage electron acceleration was put forward [23], suggesting that the electrons pre-accelerated in the BSRS process are further accelerated in the FSRS process. This mechanism requires an overlap in the velocity space for electron trapping by two plasma waves. It was found that the SRS rescattering can fill this phase velocity gap [24] and hot electrons can be produced through the interaction of a discrete spectrum of plasma waves generated from BSRS, FSRS, and rescattering. In addition, it was found that the LDI [25, 26] and anti-Stokes Langmuir decay instability (ALDI) [27, 28] following BSRS can heat electrons to higher energies because the EPW from the LDI has a slightly higher phase velocity. In order to have overlapped trapping regions for different EPWs in their phase velocities, this cascade acceleration often imposes high demands on the electron density.

On the other hand, when the EPW excited by SRS propagates in inhomogeneous plasma, the EPW wavenumber and its corresponding phase velocity changes with space and time [29-31], which may have important effects on electron trapping and acceleration. For example, for absolute SRS developed in inhomogeneous plasma near the quarter critical density, it is shown that when the excited EPWs propagate towards the turning point, some trapped electrons are accelerated by the primary EPWs as its phase velocity increases [32]. It is also found that the rescattering of SRS in inhomogeneous plasma with density less than one-fifth critical density can result in enhanced hot electron energy [33, 34].

In this work, we investigate theoretically and numerically how the evolution of EPWs excited by BSRS in plasma can affect the hot electron production generally. When the laser propagates in inhomogeneous plasma with a positive density gradient, the excited EPWs propagate with a group velocity along the direction of the plasma density rising. In the meanwhile, the wavenumber of the EPWs decreases and the phase velocity increases with time and space. The electrons trapped at early time are further accelerated to higher energies as they move from the low-density region to the high-density region following the EPWs. In our simulations, it shows that the electrons accelerated by the above heating mechanism can reach MeV energies. In contrast, when the laser propagates in plasma with a negative density gradient, the phase velocity tends to decrease with time and space, which results lower electron energy but more electrons trapped. When taking into account the ion motion, stimulated Brillouin scattering (SBS) and LDI significantly affect the development of SRS. The electron energy boosting mechanism mentioned above in plasma is effective for $k_p \lambda_D > 0.1$, where k_p and λ_D are the EPW wavenumber and electron Debye length, respectively.

Our paper is arranged as follows. In Sec. II, a model of the EPW propagation in inhomogeneous plasma is presented, which is applied to explain the evolution of EPW found in particle-in-cell (PIC) simulation. In Sec. III, numerical simulation results are presented on anomalous hot electron generation in inhomogeneous plasma via SRS due to the evolution of plasma waves. The effects of ion motion are discussed. We summarize the work in Sec. IV.

II. PROPAGATION OF AN EPW IN INHOMOGENEOUS PLASMA AND THE CHANGE OF ITS PHASE VELOCITY

To understand the hot electron generation via SRS in inhomogeneous plasma, it is necessary to understand how EPWs propagate and evolve. It has been shown before, when an EPW is excited in inhomogeneous plasma, its local wave number will change with time [31]. It is assumed that

BRS instability generates a large amplitude Langmuir wave everywhere in space, which then evolves in time.

The waves involved in SRS satisfy the frequency and wave number matching conditions,

$$\omega_0 = \omega_s + \omega_p, \quad (1)$$

$$\mathbf{k}_0 = \mathbf{k}_s + \mathbf{k}_p, \quad (2)$$

where ω and \mathbf{k} represent the frequency and wavenumber of the wave, and subscript 0, s , and p represent the incident light wave, the scattered light wave and the EPW, respectively. Each of the wave modes obeys their respective linear dispersion relation. According to the above phase matching conditions and the dispersion relations of the EPW and the electromagnetic wave, the initial wave number of the EPW excited by SRS is

$$k_p(x, 0) = c^{-1} [\sqrt{\omega_0^2 - \omega_{pe}^2} + \sqrt{(\omega_0 - \omega_{pe})^2 - \omega_{pe}^2}], \quad (3)$$

where ω_{pe} is the electron plasma frequency. Since the correction of the temperature to dispersion relationship is small here, we ignore the thermal effects in the derivation, i.e., $\omega_p \approx \omega_{pe}$. At later times, the phase of the EPW can be expressed as $\phi = \omega_p t - \int^x k_p(x, 0) dx$, and the wave number is obtained as

$$k_p(x, t) = -\frac{\partial \phi}{\partial x} = -\frac{\partial \omega_p}{\partial x} t + k_p(x, 0) \quad (4)$$

which changes with time and space. To study a specific evolution of the wavenumber, we take as an example a plasma with a linear density profile $n_e = n_0(1 + x/L)$, and the corresponding electron plasma frequency $\omega_{pe} = \omega_{pe,+} = \omega_{p0}(1 + x/L)^{1/2}$, where L is the plasma density scale length. For this case, the change of the wave number is given by $k_p(x, t) = k_{p,+}(x, t)$ with

$$k_{p,+}(x, t) = -\frac{\omega_{pe,+} t}{2(x+L)} + \frac{1}{c} \left(\sqrt{\omega_0^2 - \omega_{pe,+}^2} + \sqrt{\omega_0^2 - 2\omega_0\omega_{pe,+}} \right). \quad (5)$$

As an illustration, Eq. (5) is shown in the blue part of Fig. 1(a), where the scale length is set to $L = 300\lambda_0$ with $\lambda_0 = 2\pi c/\omega_0$ being the incident light wavelength in vacuum, and the minimum density at $x = 0$ is $n_0 = 0.19n_c$ where $n_c = \epsilon_0 m_e \omega_0^2 / e^2$ is the critical density. Consider a plasma wave located initially at the plasma density range $n_e = [0.244, 0.247]n_c$. As the EPW evolves in the inhomogeneous plasma, the wavenumber decreases with time, changing from positive, to zero, and then to negative. Although the thermal effects are ignored here, the evolution of the EPW wavenumber is actually independent of temperature and is only related to the plasma density, as will be described below.

Such a change in the wavenumber means that the phase velocity of the EPW will also change simultaneously. The EPW phase velocity is given by $v_\phi = \omega_p/k_p$. By substituting for $k_{p,+}$ from Eq. (5), we obtain the EPW phase velocity in the plasma with positive density gradient,

$$v_{\phi,+}(x, t) = \frac{\omega_{p,+}}{k_{p,+}} \approx 1 / \left[-\frac{t}{2(x+L)} + \frac{1}{c} \left(\sqrt{\frac{\omega_0^2}{\omega_{pe,+}^2} - 1} + \sqrt{\frac{\omega_0^2}{\omega_{pe,+}^2} - \frac{2\omega_0}{\omega_{pe,+}}} \right) \right], \quad (6)$$

The change of the phase velocity with time is illustrated by the blue line of Fig. 1(b). Note that the finite thickness of the line corresponds to the initial density range $[0.244, 0.247]n_c$ where electron plasma waves are assumed to be excited. As the EPW wavenumber drops in a plasma with rising density, its phase velocity rises continuously.

If the excited EPW propagates along a down-ramp density profile, such as a density profile $n_e = n_0(3/2 - x/L)$ giving $\omega_{pe} = \omega_{pe,-} = \omega_{p0}(3/2 - x/L)^{1/2}$, the evolution of wavenumber becomes $k_p(x, t) = k_{p,-}(x, t)$ with

$$k_{p,-}(x, t) \approx \frac{\omega_{pe,-}t}{3L-2x} + \frac{1}{c} \left(\sqrt{\omega_0^2 - \omega_{pe,-}^2} + \sqrt{\omega_0^2 - 2\omega_0\omega_{pe,-}} \right). \quad (7)$$

The plot of Eq. (7) is shown by the red line in Fig. 1(a), where the plasma wave is still assumed to be excited at density range $[0.244, 0.247]n_c$, and other parameters are the same as above. It can be seen that when the EPW propagates toward the lower density, its wavenumber evolves to a larger value. Similarly, the EPW phase velocity in the plasma with a down-ramp density profile can be expressed by

$$v_{\phi,-}(x, t) = \frac{\omega_{p,-}}{k_{p,-}} \approx 1 / \left[\frac{t}{3L-2x} + \frac{1}{c} \left(\sqrt{\frac{\omega_0^2}{\omega_{pe,-}^2} - 1} + \sqrt{\frac{\omega_0^2}{\omega_{pe,-}^2} - \frac{2\omega_0}{\omega_{pe,-}}} \right) \right]. \quad (8)$$

As shown in the red part of Fig. 1(b), the EPW phase velocity gradually decreases in this case.

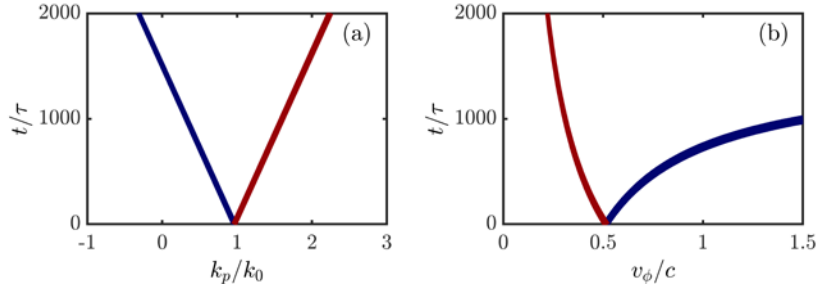


FIG.1 Evolution of the EPW wavenumber (a) and phase velocity (b) in the plasma with increasing density (blue part) and decreasing density (red part) obtained from theory.

As regard to the plasma electron temperature, it enables the EPWs to propagate out of the excitation region with a finite group velocity in an inhomogeneous plasma. In a fluid model, this can be described by the following equation for the electron density perturbation associated with the EPWs [8],

$$\frac{\partial^2 \tilde{n}_e}{\partial t^2} - 3v_e^2 \frac{\partial^2 \tilde{n}_e}{\partial x^2} + \omega_{pe}^2 \tilde{n}_e = 0, \quad (9)$$

where \tilde{n}_e is the electron density perturbation, and v_e is the electron thermal speed. In homogeneous plasma, Eq. (9) corresponds to the Bohm-Gross dispersion relation $\omega_p^2 = \omega_{pe}^2 + 3k_p^2 v_e^2$ [35]. Usually in inhomogeneous plasma, EPWs are excited locally and then propagates outside of the excitation region due to the finite electron temperature. Here, we consider a simple time-dependent model, $\tilde{n}_e = \tilde{n}_0(x, t)\exp(-i\omega t)$, and then Eq. (9) becomes

$$2i\omega \frac{\partial \tilde{n}_0}{\partial t} + 3v_e^2 \frac{\partial^2 \tilde{n}_0}{\partial x^2} + (\omega^2 - \omega_{pe}^2)\tilde{n}_0 = 0, \quad (10)$$

which is the inhomogeneous Schrödinger equation in plasma with a given electron density profile [36, 37]. Here, as we only focus on the linear propagation of EPWs, nonlinear terms and collisional effects are ignored. It can be seen from Eq. (10) that in the plasma with up-ramp density, the wavenumber of EPW evolves to $k_p = 0$ and the EPW turns at the position where the plasma frequency reaches the EPW frequency, i.e., $\omega_p = \omega_{pe}$. In the case of the density profile as $n_e = n_0(1 + x/L)$, $\omega_{pe} = \omega_{p0}(1 + x/L)^{1/2}$, the corresponding turning position for the EPW is given by $x_t(\omega_p) = (\omega_p^2/\omega_{p0}^2 - 1)L$.

Examples of the numerical solution to Eq. (10) is illustrated in Fig. 2 for different plasma electron temperatures, where the plasma density profiles are the same as Fig. 1. The initial electron density perturbation associated with an EPW is assumed to be a sinusoidal wave as $\tilde{n}_0(x, 0) = 0.05\sin(k_{p0}x)$, which is located at the initial position $x = [85, 90]\lambda_0$ with the wavenumber $k_{p0} \approx$

$0.9k_0$ and the frequency $\omega_p \approx \sqrt{0.26}\omega_0$ for the initial electron temperature $T_e = 3\text{keV}$ in Fig. 2(a). It is found that the EPWs propagate in two directions, one propagates toward the low density region and the other propagates toward the high density region. For the latter case, the EPW will turn at the position when $k_p = 0$ for the wavenumber of the EPW. In this case, the calculated position of the turning point is approximately at $x_t(\omega_p) \approx 110\lambda_0$, which is roughly in line with the results in Fig. 2(a).

Now it is clear that the evolution of the plasma wavenumber k_p can be attributed to two factors, one is due to the density inhomogeneity as described by Eqs. (5) and (7). The other is due to the finite electron temperature as described by Eq. (9) or Eq. (10). A finite electron temperature introduces a finite group velocity of the EPW. To examine which factor plays a dominant role for the plasma wavenumber evolution, we have carried out simulations with different electron temperatures while keeping the plasma density profile and initial density perturbations fixed, as shown in Figs. 2(b) and 2(c). It can be found that when the initial temperature changes, the turning position of the EPW changes accordingly, but the corresponding time is almost the same, all around $t = 1500\tau$ represented by the white dashed line. This is what estimated by Eq. (5). The change of turning position is caused by different magnitudes of the group velocity, which make the EPWs propagate different distances in the same time. This suggests that the evolution of the wavenumber in time is mainly determined by the plasma density distribution in space, and to lesser extent by the electron temperature.

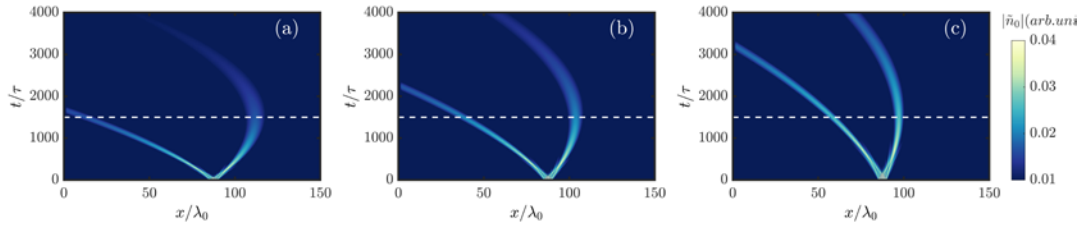


FIG. 2 Spatiotemporal plots of the EPWs propagation in inhomogeneous plasma obtained from Eq. (10), for initial electron temperatures $T_e = 3\text{keV}$ (a), $T_e = 2\text{keV}$ (b), $T_e = 1\text{keV}$ (c). In each plot, two EPW wave packets are excited, one propagates to the low density region and the other one to the high density region until $k_p = 0$ (or the group velocity reduces to zero) and then turns back to the low density region. Space and time are normalized to the laser wavelength and period, respectively.

To validate the above features of EPW propagation in inhomogeneous plasma obtained based upon theoretical analysis, we have carried out one-dimensional particle-in-cell (PIC) simulations with the code EPOCH [38]. In the following two simulations, a laser pulse with wavelength $\lambda_0 = 0.351\mu\text{m}$ and duration $t = 580\text{fs}$ is incident into an inhomogeneous plasma slab from the left and right boundaries, respectively. The density profile is assumed to vary linearly with space as $n_e = 0.19n_c(1 + x/300)$, which is the same as in Fig. 1. Look first at the case in Fig 3 of laser incidence from the left side of the plasma, corresponding to the laser propagation along an up-ramp density profile. BSRS develops most efficiently near the quarter-critical density. The excited EPWs propagates forward due to the finite electron temperature, and then turn at a higher density, as shown in Fig. 3(a). Around the plasma density $n_0 = 0.24n_c$ and at the initial electron temperature $T_e = 3\text{keV}$, the frequency of the EPW excited by BSRS can be estimated to be $\omega_p \approx \sqrt{0.26}\omega_0$. The theoretical position of the turning point is at $x_t \approx 110\lambda_0$, which is the same as in Fig. 2(a) for the

wave packet propagating to the high-density region. Therefore, the simulation results in Fig. 3(a) for the trajectory of the EPW packet are well in agreement with that of the inhomogeneous Schrödinger equation (10).

Another feature of the EPW evolution is found in the wave number due to the plasma density inhomogeneity as described by Eq. (5), which is also found in the PIC simulation. Figures 3(b) and 3(c) show the spectra of the electrostatic fields found in the time windows of $[500,1000]\tau$ and $[2500,3000]\tau$, respectively. It is obvious that the wavenumber decreases from positive in Fig. 3(b) to negative in Fig. 3(c), while the EPW frequency remain almost constant. To see the evolution of the wavenumber clearly, we have plotted the temporal evolution of the EPW wavenumber in Fig. 3(d). It is obvious that the wavenumber reduces with time until $k_p = 0$ at the turning point at about $t = 2000\tau$. Afterwards, $k_p < 0$ with its absolute value increases with time. This is consistent with the trend in Fig. 1(a). Taking into account the time of laser propagation and SRS development in the simulation, it is found that the time of the EPW turning found in the simulation is in agreement with that predicted by the theory model shown above. From Fig. 3(d), as the plasma frequency changes little with time, the phase velocity changes from $0.55c$ to $+\infty$ during $[500,1500]\tau$.

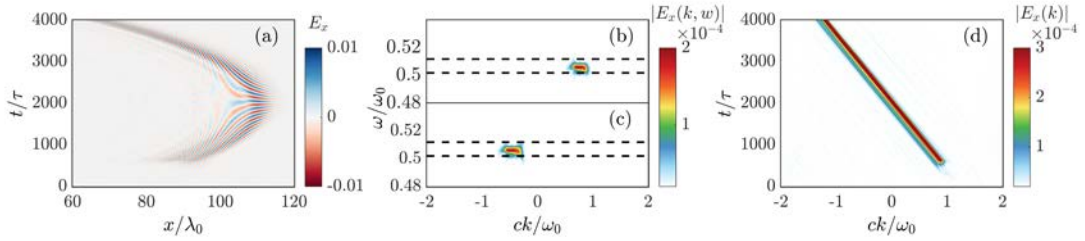


FIG. 3 PIC simulation results for the evolution of the EPW excited by SRS when a laser pulse is incident from the left boundary of the simulation box. (a) and (d) Time-space and time-wavenumber distributions of the EPW. (b) and (c) Wavenumber-frequency distributions of the EPW in the time windows $[500, 1000]\tau$ and $[2500, 3000]\tau$, respectively. The two black dash lines corresponds to the frequency of the EPWs excited at $0.24n_c$ and $0.25n_c$.

We next study the same density profile setting, but now the laser is incident from the right side of the plasma, which corresponds to the laser /EPW propagation along a down-ramp density profile. One can see in Fig. 4(a) that the EPW keeps propagating to the left boundary without turning, which is consistent with the EPW mode propagating to the left as shown in Fig. 2. Also, the magnitude of the wavenumber will continue to increase with time as shown in Figs. 4(b)-4(d). In this case, the phase velocity of the EPW will continue to decrease. This implies that more electrons could be trapped with time.

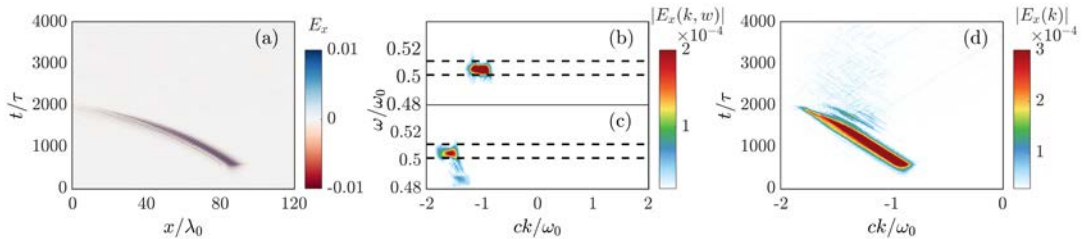


FIG. 4 Simulation results when the laser is incident from the right boundary, i.e., the laser propagation along a down-ramp density profile. (a) and (d) Time-space and time-wavenumber distributions of EPW. (b) and (c) Wavenumber-frequency distributions of EPW in the time windows $[500, 1000]\tau$ and $[1500, 2000]\tau$, respectively.

III. HOT ELECTRONS ACCELERATED IN THE EVOLVING EPWS

A. Electron trapping conditions and energy gain in EPWs in homogeneous plasma

Our analysis above suggests that the EPW phase velocity changes continuously with time and space in inhomogeneous plasma. In plasma with an up-ramp density profile, the EPW phase velocity increases with time within a certain time window. Thus, some trapped electrons could be continuously accelerated to high energy. To examine this, let us first consider the electron trapping conditions in homogeneous thermal plasma. When the thermal velocity of the electron v_e and the phase velocity of the EPW v_ϕ are comparable, a significant number of electrons will be trapped by the EPW, resulting in the energy transfer from the wave to some trapped electrons. In the nonrelativistic limit, the velocity of electrons accelerated by EPW is related to v_ϕ and the trapping width v_{tr} , that is, the trapped electrons oscillate between $v_{max} = v_\phi \pm v_{tr}$.

We analyze the evolution of the phase velocity of the EPW excited by the SRS in Fig. 1(b). When the EPW wavenumber drops in plasma with the up-ramp density profile, its phase velocity rises continuously. Then, the electrons trapped at the beginning can be continuously accelerated by the evolved EPWs to higher energies. In the opposite case, the EPW phase velocity gradually decreases in plasma with the down-ramp density profile. This means that the evolved plasma wave can trap a larger number of low-speed electrons.

Regarding the trapping width, it is related to the EPW amplitude and wavenumber by $v_{tr} = 2\sqrt{eE_{pe}/(m_e k)}$, as a balance between kinetic energy $m_e v_{tr}^2/2$ and potential energy eE_{pe}/k in the frame of the EPW wave front. In the process of propagating and evolving, although the amplitude of the EPW is affected by damping and decreases, the wavenumber in the denominator of the above equation has a more pronounced change. If the EPW propagates in plasma with the up-ramp density profile, the trapping width increases rapidly as the wavenumber decreases, and there will be a relatively wide trapping range in the velocity distribution.

The effect of the wavenumber variation is evident both for the phase velocity and the trapping width. In the following subsections, we present a set of simulations to show the effects of plasma wavenumber evolution on electron acceleration in inhomogeneous plasma.

B. Electron acceleration in inhomogeneous plasma from PIC simulations

In Fig. 5, we first consider Case 1 with an up-ramp density profile and with fixed ions, which excludes the interference of other LPs such as SBS and LDI. The key parameters used in this case are listed below. The laser has the intensity $I_0 = 4.4 \times 10^{15} \text{ W/cm}^2$, the wavelength $\lambda_0 = 0.351 \mu\text{m}$, and a semi-infinite duration. The simulation box has a length of $200\lambda_0$ along the longitudinal x-axis and the plasma is distributed with a density profile $n_e = 0.23n_c(1 + x/800)$, as shown in Fig. 5(a), where the quarter critical density is found at $x \approx 70\lambda_0$. The initial electron temperature is $T_e = 3\text{keV}$.

The high density and large density gradient used in our simulations make rescattering of SRS and FSRS less likely, so only BSRS is considered here. At the density $n_e = 0.23n_c$, the wavenumber of the EPW excited by BSRS is approximately $k_p \approx 1.02k_0$. From Fig. 5(b), we can see that the initial wavenumber of the EPW excited via BSRS is slightly larger than k_0 , which is consistent with the theoretical value. The EPW propagates forward with the decreasing wavenumber and gradually decay over a distance.

Near the density $0.23n_c$, the EPW frequency is calculated to be $\omega_p = 0.50\omega_0$, then the phase velocity obtained is approximately at $v_\phi \approx 0.49c$. The amplitude of the EPW in the simulation is roughly about $eE_{pe}/m_e\omega_0c = 0.06$, and the trapping width is estimated to be $v_{tr} \approx 0.49c$. The theoretical estimate agrees with the PIC simulation results at the early stage as illustrated in Fig. 5(c). Afterwards, the excited EPW propagates to the right and its wavenumber has evolved to a smaller value with time. As a result, a higher phase velocity is found and, in the meanwhile, the trapping width increases due to the reduction of the wavenumber. Subsequently the trapped electrons are accelerated to higher momenta, as shown in Fig. 5(d). Figure 5(e) illustrated the electron energy spectra at different time. The electrons are accelerated to much higher energy at a later stage ($t = 3000\tau$) than that at an earlier stage ($t = 1000\tau$). The slope of the hot electron tail at $t = 3000\tau$ is fit using a temperature of $T_e \approx 935\text{keV}$. This agrees with the fact that the EPW phase velocities evolve to high values even up to superluminal. Our simulation results suggest that the wavenumber evolution of the EPW in plasma with an up-ramp density profile leads to the production of a large number of hot electrons with high energy.

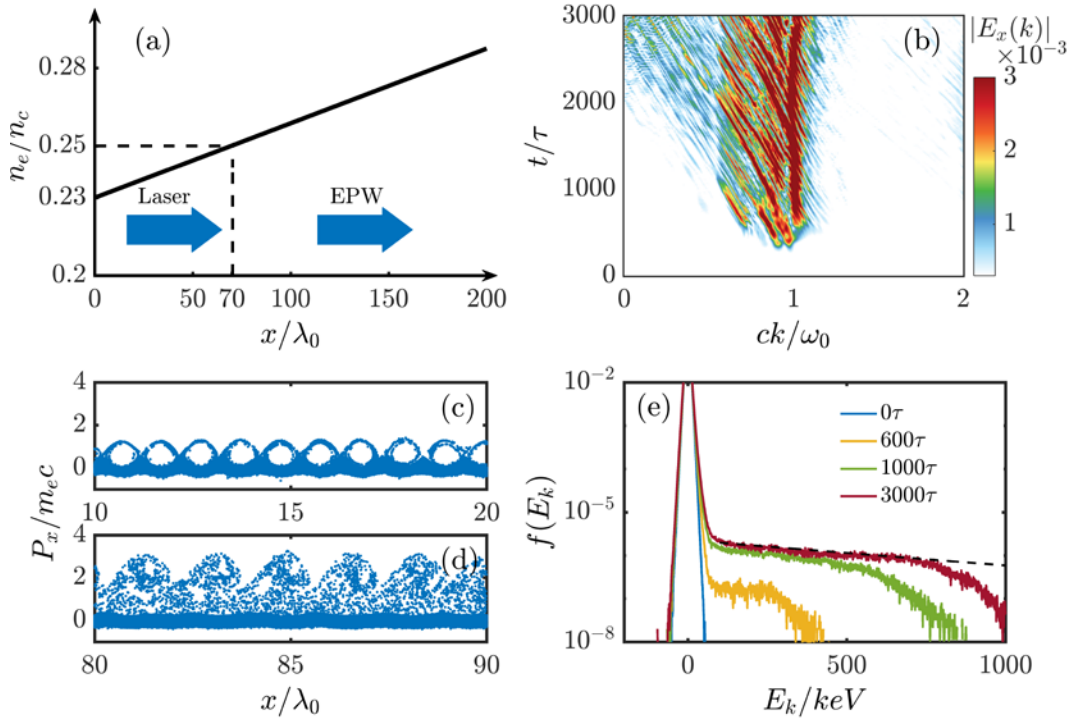


FIG. 5 Evolution of the EPW wavenumber and electron phase space in Case 1. (a) The up-ramp density profile used in this simulation. (b) The temporal evolution of the EPW wavenumber. The phase space distributions of electrons in $[10, 20]\lambda_0$ (c) and in $[80, 90]\lambda_0$ at $t = 2000\tau$ (d). (e) Energy distributions of electrons at different time.

As a comparison, we consider in Fig. 6 the excited EPW propagates along a down-ramp density in Case 2, where the density profile is shown in Fig. 6(a). In this case, its wavenumber gradually increases and the phase velocity decreases according to Sec. II, which is agreement with PIC simulation as shown in Fig. 6(b). The phase velocity at the beginning is the maximum phase velocity, which tends to decrease with time. This implies that more low energy electrons can be trapped by EPWs as illustrated in Figs. 6(c) and 6(d). From Fig. 6(e), the slope of the hot electron tail at $t = 2000\tau$ is fit using a temperature $T_e \approx 217\text{keV}$, which is close to the theoretical value calculated by

the three-wave coupling conditions. Comparing the electron energy spectra at $t = 1000\tau$ and 2000τ , more low-speed electrons are found to be trapped at $t = 2000\tau$. The comparison of Case 1 and 2 demonstrates that the evolution of the plasma wave leads to dramatically different features of electron acceleration due to their different evolution of the plasma wavenumbers in up-ramp and down-ramp density profiles.

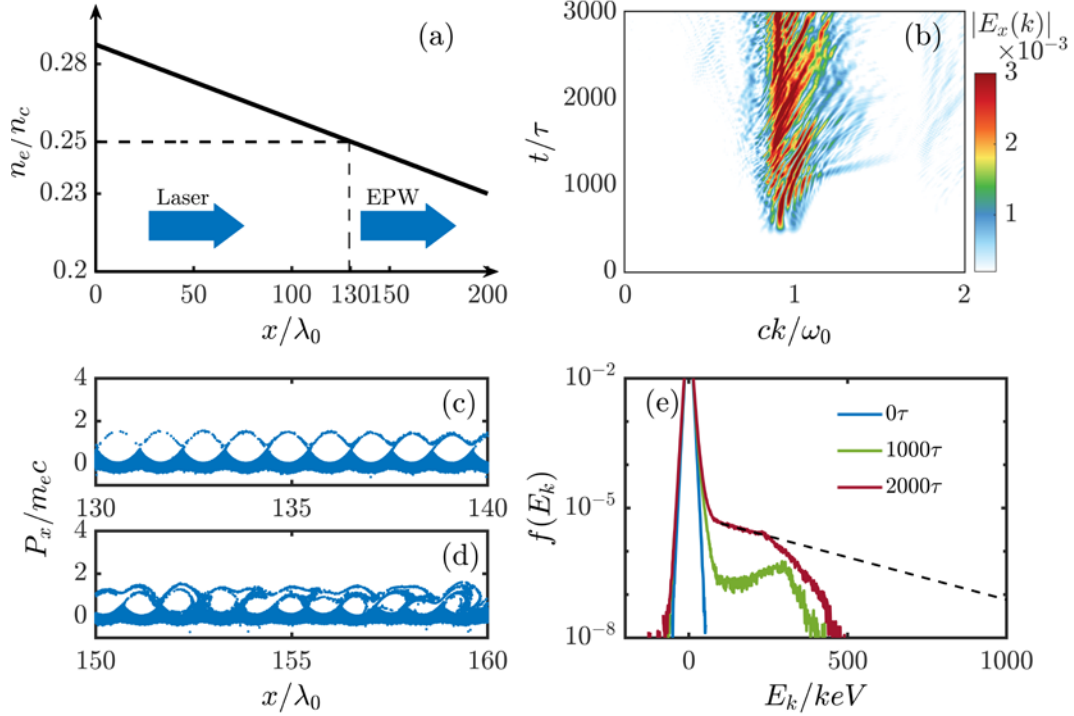


FIG. 6 Evolution of the EPW wavenumber and electron phase space in Case 2. (a) The down-ramp density profile used in this simulation. (b) The temporal evolution of the EPW wavenumber. The phase space of electrons in $[130,140]\lambda_0$ (c) and in $[150,160]\lambda_0$ at $t = 2000\tau$ (d). (e) Energy distributions of electrons at different time.

C. Effects of ion motion on electron acceleration

When we consider the ion motion, new types of LPs associated with ion motion will take place and electron acceleration processes gets more involved. An important parameter in the discussion of nonlinear EPW regimes is a dimensionless parameter $k_p \lambda_D$ [26], where k_p is the EPW wavenumber and λ_D is the electron Debye length. In the kinetic regime with $k\lambda_D \geq 0.29$, it is prone to get the frequency-broadened spectrum associated with electron trapping. However, in this regime, phenomena such as wavebreaking are more likely to occur [39]. In the fluid regime with $k\lambda_D < 0.29$, LDI will take place, which could be one of the saturation mechanisms of SRS. Meanwhile, the decaying EPW from LDI has a smaller wavenumber, so there will be a higher phase velocity to heat trapped electrons to a higher temperature. Moreover, if the plasma wavenumber is smaller, $k\lambda_D < 0.1$, EPW collapse and strong turbulence is the dominant nonlinearity [40], where the EPW is getting trapped in ion density cavities and does not reach any stable state. Given the above consideration, we focus on the parameter regime with $0.1 < k\lambda_D < 0.29$.

The parameters in the following case are similar to those in Fig.5 for the laser and plasma density profile, except for the ions motion and initial electron temperature. Assuming the ions to be protons, we take the ion to electron mass ratio to be $m_i/m_e = 1836$ in the simulation. To reduce

the impact of EPW collapse, the electron temperature is raised to 5keV, so that the SRS remains in the fluid regime for $k\lambda_D = 0.2$ without strong turbulence. As illustrated in Fig. 7, the reflectivity due to SRS is more volatile in the ion-mobile case than the ion-fixed case at the early stage. Later, the generation of LDI and the development of SBS act to quench SRS, which suppress the excitation of EPW. As a whole, the level of SBS is relatively low in the early stage, so we still focus mainly on the SRS and its subsequent decay instability.

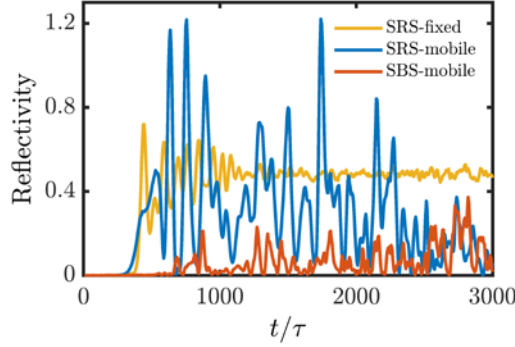


FIG. 7 Instantaneous reflectivity due to SRS in the ion-fixed case (yellow line), as well as due to SRS and SBS in the ion-mobile case (blue and red line) diagnosed at the left boundary.

Figure 8 demonstrates the spectrum of the EPW and hot electron energy spectra for ion-mobile case. It is obvious that LDI has been already excited in this case as shown in Fig. 8(a), where the signal of the positive wavenumber is mainly generated by SRS and the negative part is generated by LDI of SRS. The LDI-excited secondary EPW have smaller wavenumber and frequency than the primary EPW, which is precisely determined by the three-wave coupling conditions of LDI. Figure 8(b) illustrate the evolution of the forward and backward propagating EPW. The SRS started to develop around $t = 290\tau$, and LDI appeared at time after $t = 500\tau$. Although the EPWs are not so stable under the impact of various nonlinear effects, there is still a clear trend of wavenumber evolution.

Because of the backward propagating EPW produced by LDI, some electrons are accelerated in the backward direction. Figure 8(c) shows that electrons are accelerated both in the forward and backward directions to a comparable level. Since the SRS develops relatively early, there is already a pronounced heating of electrons at $t = 500\tau$ in the positive direction, and no obvious heating in the negative direction at that time. At a later time $t = 1000\tau$, the EPWs evolve to higher phase velocities, accelerating the electrons up to about 500keV, where the hot electron tail has a temperature around $T_e \approx 564\text{keV}$ in the positive direction. Further later in time, as the EPW begin to decay, the heating temperature decreases. However, due to its slower development, the backward EPW traps a larger number of electrons at $t = 2000\tau$. Overall, when ions are mobile, the energy of electrons heated by EPW is not as high as when ions are fixed due to various nonlinearities, but the EPW evolution as well as electron acceleration is still present.

Although the results shown above are all near the quarter-critical density, electron acceleration due to the EPW evolution also plays a role in low density and low temperature plasma. Simulations not presented here also show that the EPW evolution is still evident in inhomogeneous plasma with density below $0.2n_c$, and high-energy electrons are generated beyond the initial theoretical value.

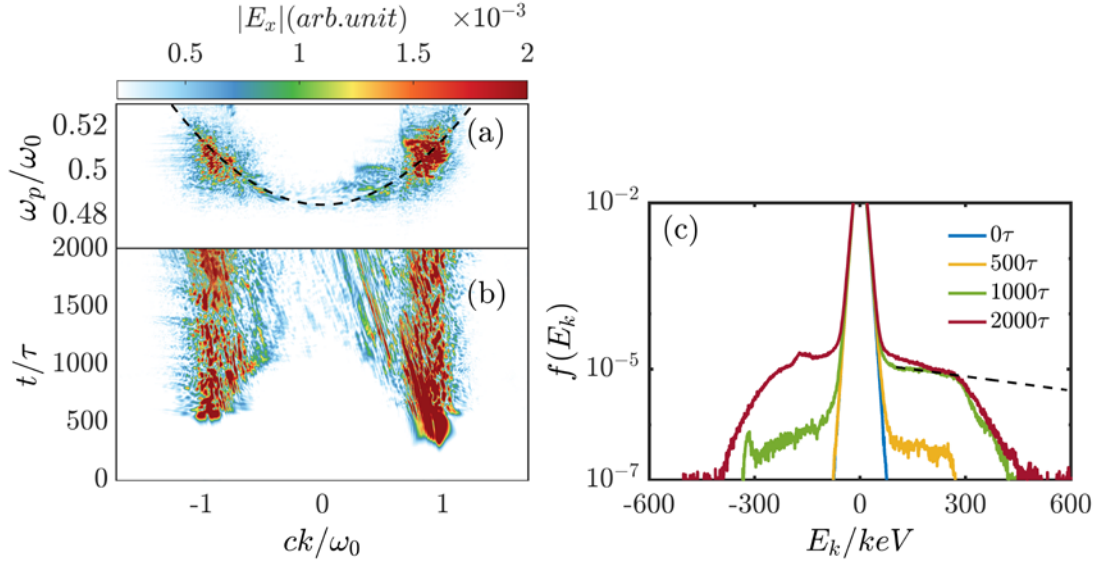


FIG. 8 The simulation results of Case 3. (a) Wavenumber-frequency distributions of the EPW during $[0, 2000]\tau$. (b) The temporal evolution of the forward propagating EPWs. (c) The electron energy spectrum at different time.

IV. CONCLUSIONS

The evolution of the EPW initially excited by the SRS and subsequent electron acceleration in an inhomogeneous plasma are investigated theoretically and numerically. It is found that the EPW excited by SRS can propagate out of the resonant region due to the finite electron temperature. Besides, the EPW wavenumber changes with time and space due to the density inhomogeneity. The evolution of EPWs in plasma with an up-ramp density profile is dramatically different from that with a down-ramp density profile. In the former case, the EPW wavenumber becomes smaller and the phase velocity gradually increases up to superluminal, driving anomalous electron acceleration even up to the order of MeV.

In the case when ion motion is considered, the situation is more complicated due to the coupling with the development of SBS, LDI as well as EPW collapse. These change the saturation level of SRS and limits the time the EPW remains stable. In spite of all these factors, a clear wavenumber evolution is observed in the simulations and the electron temperature is also increased to a high level.

The anomalous acceleration mechanism studied here may also be found in other LPI process involving EPWs as product waves, such as the sideward-SRS and two-plasmon decay. The excited EPW evolves and continues to transfer energy to the electrons, releasing a large number of suprathermal electrons. The mechanism presented in this work provides a possible explanation for high-energy electron generation observed in experiments.

Acknowledgements

This work is supported by the Strategic Priority Research Program of Chinese Academy of Sciences (Grant No. XDA25050100), the National Natural Science Foundation of China (Grant Nos. 11991074, 11975154, 12135009 and 12005287).

REFERENCES

- ¹R. Betti and O.A. Hurricane, "Inertial-confinement fusion with lasers," *Nature Physics* 12, 435-448 (2016).
- ²K. Lan, "Dream fusion in octahedral spherical hohlraum," *Matter and Radiation at Extremes* 7, 055701 (2022).
- ³E.M. Campbell, V.N. Goncharov, T.C. Sangster, S.P. Regan, P.B. Radha, R. Betti, J.F. Myatt, D.H. Froula, M.J. Rosenberg, I.V. Igumenshchev, et al., "Laser-direct-drive program: Promise, challenge, and path forward," *Matter and Radiation at Extremes* 2, 37-54 (2017).
- ⁴D.S. Montgomery, "Two decades of progress in understanding and control of laser plasma instabilities in indirect drive inertial fusion," *Physics of Plasmas* 23, 055601 (2016).
- ⁵R.K. Kirkwood, J.D. Moody, J. Kline, E. Dewald, S. Glenzer, L. Divol, P. Michel, D. Hinkel, R. Berger, E. Williams, et al., "A review of laser-plasma interaction physics of indirect-drive fusion," *Plasma Physics and Controlled Fusion* 55, 103001 (2013).
- ⁶S.P. Regan, D.K. Bradley, A.V. Chirikikh, R.S. Craxton, D.D. Meyerhofer, W. Seka, R.W. Short, A. Simon, R.P.J. Town, B. Yaakobi, et al., "Laser-plasma interactions in long-scale-length plasmas under direct-drive National Ignition Facility conditions," *Physics of Plasmas* 6, 2072-2080 (1999).
- ⁷V. Tikhonchuk, Y.J. Gu, O. Klimo, J. Limpouch and S. Weber, "Studies of laser-plasma interaction physics with low-density targets for direct-drive inertial confinement schemes," *Matter and Radiation at Extremes* 4, 045402 (2019).
- ⁸W.L. Kruer, *The Physics of Laser Plasma Interaction*(Addison-Wesley, New York, 1988).
- ⁹C.S. Liu, V.K. Tripathi and B. Eliasson, *High-Power Laser-Plasma Interaction*(Cambridge University Press, Cambridge, 2019).
- ¹⁰M.J. Rosenberg, A.A. Solodov, W. Seka, R.K. Follett, J.F. Myatt, A.V. Maximov, C. Ren, S. Cao, P. Michel, M. Hohenberger, et al., "Stimulated Raman scattering mechanisms and scaling behavior in planar direct-drive experiments at the National Ignition Facility," *Physics of Plasmas* 27, 042705 (2020).
- ¹¹A.A. Solodov, M.J. Rosenberg, W. Seka, J.F. Myatt, M. Hohenberger, R. Epstein, C. Stoeckl, R.W. Short, S.P. Regan, P. Michel, et al., "Hot-electron generation at direct-drive ignition-relevant plasma conditions at the National Ignition Facility," *Physics of Plasmas* 27, 052706 (2020).
- ¹²Y. Zhao, S. Weng, M. Chen, J. Zheng, H. Zhuo and Z. Sheng, "Stimulated Raman scattering excited by

- incoherent light in plasma," *Matter and Radiation at Extremes* 2, 190-196 (2017).
- ¹³H.H. Ma, X.F. Li, S.M. Weng, S.H. Yew, S. Kawata, P. Gibbon, Z.M. Sheng and J. Zhang, "Mitigating parametric instabilities in plasmas by sunlight-like lasers," *Matter and Radiation at Extremes* 6, 055902 (2021).
- ¹⁴Y. Guo, X. Zhang, D. Xu, X. Guo, B. Shen and K. Lan, "Suppression of stimulated Raman scattering by angularly incoherent light, towards a laser system of incoherence in all dimensions of time, space, and angle," *Matter and Radiation at Extremes* 8, 035902 (2023).
- ¹⁵K.L. Baker, R.P. Drake, B.S. Bauer, K.G. Estabrook, A.M. Rubenchik, C. Labaune, H.A. Baldis, N. Renard, S.D. Baton, E. Schifano, et al., "Observation of the Langmuir decay instability driven by stimulated Raman scattering," *Physics of Plasmas* 4, 3012-3020 (1997).
- ¹⁶S. Depierreux, C. Labaune, J. Fuchs, D. Pesme, V.T. Tikhonchuk and H.A. Baldis, "Langmuir Decay Instability Cascade in Laser-Plasma Experiments," *Physical Review Letters* 89, 045001 (2002).
- ¹⁷D.A. Russell, D.F. Dubois and H.A. Rose, "Nonlinear saturation of stimulated Raman scattering in laser hot spots," *Physics of Plasmas* 6, 1294-1317 (1999).
- ¹⁸H.X. Vu, D.F. Dubois and B. Bezzerides, "Kinetic inflation of stimulated Raman backscatter in regimes of high linear Landau damping," *Physics of Plasmas* 9, 1745-1763 (2002).
- ¹⁹W.L. Kruer, K. Estabrook, B.F. Lasinski and A.B. Langdon, "Raman backscatter in high temperature, inhomogeneous plasmas," *The Physics of Fluids* 23, 1326-1329 (1980).
- ²⁰H. Figueroa, C. Joshi, H. Azechi, N.A. Ebrahim and K. Estabrook, "Stimulated Raman scattering, two-plasmon decay, and hot electron generation from underdense plasmas at 0.35 μm ," *The Physics of Fluids* 27, 1887-1896 (1984).
- ²¹K. Estabrook, W.L. Kruer and B.F. Lasinski, "Heating by Raman Backscatter and Forward Scatter," *Physical Review Letters* 45, 1399-1403 (1980).
- ²²K. Estabrook and W.L. Kruer, "Theory and simulation of one-dimensional Raman backward and forward scattering," *The Physics of Fluids* 26, 1892-1903 (1983).
- ²³P. Bertrand, A. Ghizzo, S.J. Karttunen, T.J.H. Pättikangas, R.R.E. Salomaa and M. Shoucri, "Two-stage electron acceleration by simultaneous stimulated Raman backward and forward scattering," *Physics of Plasmas* 2, 3115-3129 (1995).
- ²⁴B.J. Winjum, J.E. Fahlen, F.S. Tsung and W.B. Mori, "Anomalous Hot Electrons due to Rescatter of Stimulated Raman Scattering in the Kinetic Regime," *Physical Review Letters* 110, 165001 (2013).

- 25**J.L. Kline, D.S. Montgomery, B. Bezzerides, J.A. Cobble, D.F. Dubois, R.P. Johnson, H.A. Rose, L. Yin and H.X. Vu, "Observation of a Transition from Fluid to Kinetic Nonlinearities for Langmuir Waves Driven by Stimulated Raman Backscatter," *Physical Review Letters* 94, 175003 (2005).
- 26**J.L. Kline, D.S. Montgomery, L. Yin, D.F. Dubois, B.J. Albright, B. Bezzerides, J.A. Cobble, E.S. Dodd, D.F. Dubois, J.C. Fernández, et al., "Different $k\lambda_D$ regimes for nonlinear effects on Langmuir waves," *Physics of Plasmas* 13, 055906 (2006).
- 27**Q.S. Feng, R. Aboushelbaya, M.W. Von Der Leyen, B.T. Spiers, R.W. Paddock, I. Ouatu, R. Timmis, R.H.W. Wang, L.H. Cao, Z.J. Liu, et al., "Suprathermal electrons from the anti-Stokes Langmuir decay instability cascade," *Physical Review E* 105, 045208 (2022).
- 28**Q.S. Feng, Z.J. Liu, C.Y. Zheng, C.Z. Xiao, Q. Wang, H.C. Zhang, L.H. Cao and X.T. He, "Anti-Stokes scattering and Stokes scattering of stimulated Brillouin scattering cascade in high-intensity laser-plasma interaction," *Plasma Physics and Controlled Fusion* 59, 075007 (2017).
- 29**Z.-M. Sheng, K. Mima, J. Zhang and H. Sanuki, "Emission of Electromagnetic Pulses from Laser Wakefields through Linear Mode Conversion," *Physical Review Letters* 94, 095003 (2005).
- 30**Z.-M. Sheng, K. Mima and J. Zhang, "Powerful terahertz emission from laser wake fields excited in inhomogeneous plasmas," *Physics of Plasmas* 12, 123103 (2005).
- 31**X.Y. Jiang, S.M. Weng, H.H. Ma, X.F. Li, C.F. Wu, Z. Liu, Y. Zhao, M. Chen and Z.M. Sheng, "Broadband electromagnetic emission via mode conversion mediated by stimulated Raman scattering in inhomogeneous plasma," *Physics of Plasmas* 30, 075007 (2023).
- 32**Q. Wang, W. Rozmus and J.F. Myatt, "Nonlinear development of absolute Raman backscatter in ignition-scale direct-drive coronal conditions," *Physics of Plasmas* 28, 122711 (2021).
- 33**Y. Zhao, Z. Sheng, S. Weng, S. Ji and J. Zhu, "Absolute instability modes due to rescattering of stimulated Raman scattering in a large nonuniform plasma," *High Power Laser Science and Engineering* 7, e20 (2019).
- 34**Y. Ji, C.-W. Lian, R. Yan, C. Ren, D. Yang, Z.-H. Wan, B. Zhao, C. Wang, Z.-H. Fang and J. Zheng, "Convective amplification of stimulated Raman rescattering in a picosecond laser plasma interaction regime," *Matter and Radiation at Extremes* 6, 015901 (2021).
- 35**D. Bohm and E.P. Gross, "Theory of Plasma Oscillations. A. Origin of Medium-Like Behavior," *Physical Review* 75, 1851-1864 (1949).
- 36**G.J. Morales, Y.C. Lee and R.B. White, "Nonlinear Schrödinger-Equation Model of the Oscillating Two-Stream Instability," *Physical Review Letters* 32, 457-460 (1974).

- ³⁷G.J. Morales and Y.C. Lee, "Ponderomotive-Force Effects in a Nonuniform Plasma," *Physical Review Letters* 33, 1016-1019 (1974).
- ³⁸T.D. Arber, K. Bennett, C.S. Brady, A. Lawrence-Douglas, M.G. Ramsay, N.J. Sircombe, P. Gillies, R.G. Evans, H. Schmitz, A.R. Bell, et al., "Contemporary particle-in-cell approach to laser-plasma modelling," *Plasma Physics and Controlled Fusion* 57, 113001 (2015).
- ³⁹H.H. Ma, C.F. Wu, S.M. Weng, S.H. Yew, Z. Liu, X.F. Li, S. Kawata, Z.M. Sheng and J. Zhang, "Simulations of laser plasma instabilities using a particle-mesh method," *Plasma Physics and Controlled Fusion* 63, 095005 (2021).
- ⁴⁰D.F. Dubois, D.A. Russell, P.Y. Cheung and M.P. Sulzer, "High-power high-frequency-induced Langmuir turbulence in the smooth ionosphere at Arecibo. I. Theoretical predictions for altitude-resolved plasma line radar spectra," *Physics of Plasmas* 8, 791-801 (2001).